Arctic sea-ice decline archived by multicentury annual-resolution record from crustose coralline algal proxy

Jochen Halfar[a,1], Walter H. Adey[b], Andreas Kronz[c], Steffen Hetzinger[d], Evan Edinger[e], and William W. Fitzhugh[f]

[a]Department of Chemical and Physical Sciences, University of Toronto at Mississauga, Mississauga, ON, Canada L5L 1C6; [b]Department of Botany, MRC 164, Smithsonian Institution, Washington, DC 20560; [c]Geowissenschaftliches Zentrum, Universität Göttingen, D-37077 Göttingen, Germany; [d]Paläo-Ozeanographie, Ozeanzirkulation und Klimadynamik, GEOMAR Helmholtz-Zentrum für Ozeanforschung Kiel, Wischhofstr. 1-3, 24148 Kiel, Germany; [e]Department of Geography, Memorial University of Newfoundland, St. John's, NL, Canada A1B 3X9; and [f]Department of Anthropology, National Museum of Natural History, MRC 112, Smithsonian Institution, Washington, DC 20560

Edited by John M. Hayes, Woods Hole Oceanographic Institution, Woods Hole, MA, and approved October 18, 2013 (received for review July 24, 2013)

Northern Hemisphere sea ice has been declining sharply over the past decades and 2012 exhibited the lowest Arctic summer sea-ice cover in historic times. Whereas ongoing changes are closely monitored through satellite observations, we have only limited data of past Arctic sea-ice cover derived from short historical records, indirect terrestrial proxies, and low-resolution marine sediment cores. A multicentury time series from extremely long-lived annual increment-forming crustose coralline algal buildups now provides the first high-resolution in situ marine proxy for sea-ice cover. Growth and Mg/Ca ratios of these Arctic-wide occurring calcified algae are sensitive to changes in both temperature and solar radiation. Growth sharply declines with increasing sea-ice blockage of light from the benthic algal habitat. The 646-y multisite record from the Canadian Arctic indicates that during the Little Ice Age, sea ice was extensive but highly variable on subdecadal time scales and coincided with an expansion of ice-dependent Thule/Labrador Inuit sea mammal hunters in the region. The past 150 y instead have been characterized by sea ice exhibiting multidecadal variability with a long-term decline distinctly steeper than at any time since the 14th century.

Sea ice plays an important role in the global climate system because it influences albedo, heat and gas exchange, freshwater budget, ocean stratification, and deep water mass formation, among other ocean characteristics (1, 2). Presently, there is great concern that with ongoing warming, Arctic sea-ice decline is accelerating at an unprecedented pace not seen in at least the past 1,450 y (3). Sea-ice cover (SIC) is a sensitive parameter characterized by high variability in space and time (1) and analysis of sea-ice extent on a regional basis reveals that positive and negative anomalies in different sectors of the Arctic often occur simultaneously (4). Early 20th century Northern Hemisphere warming and sea-ice decline were mainly concentrated on the Atlantic portion of the Arctic with focal points in the Labrador Sea and Greenland, whereas mid–late 20th century sea-ice loss was most evident in the Russian Arctic (5–7). Modeling studies indicate that this differential sea-ice decline has likely been caused by Atlantic inflow variability into the Arctic (5, 8) and at least in part driven by the North Atlantic Oscillation (NAO) (7).

However, the SIC–atmosphere system is especially difficult to model with only a short observational record available. Instrumental data from satellite observations have been recorded only since the late 1970s when anthropogenic effects were likely already overprinting the natural climate system. Longer-term data from historical observations are far less dependable, because coverage is patchy and reliability sometimes uncertain. For a better understanding of long-term sea-ice variability, both in space and time, a network of high-resolution multicentury or millennial-scale sea-ice data derived from proxy records are needed (3, 9). High-resolution terrestrial archives such as tree rings, varved lake sediments, and ice-core records have been used to document the atmospheric forcing of, or atmospheric response to, changes in sea-ice cover (3). Unfortunately, the relationship of terrestrial records with sea ice is not direct and marine SIC proxy records are therefore preferable. Existing marine SIC proxy records are derived from biological, chemical, or sedimentological tracers preserved in marine sediment cores. Most sediment cores, however, suffer from poor temporal resolution, generally not exceeding decadal or even centennial scales (1, 10). Hence, to date, marine proxy sea-ice records are not able to resolve high-frequency climate oscillations during the past millennium such as the NAO that are crucial for understanding recent dramatic changes in SIC.

The yearly increment-forming photoautotrophic crustose coralline alga *Clathromorphum compactum*, which is widely distributed across Subarctic and Arctic coastal areas of the Northern Hemisphere (11), provides much needed annually resolved in situ sea-ice records spanning more than half a millennium. *Clathromorphum* has been calibrated as a proxy archive (12) and was subsequently used to generate multicentury-scale climate records from extratropical oceans (13). Photosynthetic *Clathromorphum* buildups have a fixed mode of life on rocky substrate and can therefore monitor and record light reaching the shallow seafloor in their high-Mg calcite skeleton. Life spans of individual plants are only limited by physical disturbance events on the seafloor, such as extreme grazing, seafloor instability, or iceberg scouring (11). Here we report on recently discovered

Significance

The most concerning example of ongoing climate change is the rapid Arctic sea-ice retreat. While just a few years ago ice-free Arctic summers were expected by the end of this century, current models predict this to happen by 2030. This shows that our understanding of rapid changes in the cryosphere is limited, which is largely due to a lack of long-term observations. Newly discovered long-lived algae growing on the Arctic seafloor and forming tree-ring–like growth bands in a hard, calcified crust have recorded centuries of sea-ice history. The algae show that, while fast short-term changes have occurred in the past, the 20th century exhibited the lowest sea-ice cover in the past 646 years.

Author contributions: J.H. and W.H.A. designed research; J.H., W.H.A., A.K., and W.W.F. performed research; W.H.A., A.K., and E.E. contributed new reagents/analytic tools; J.H., A.K., and S.H. analyzed data; and J.H. wrote the paper.

The authors declare no conflict of interest.

This article is a PNAS Direct Submission.

Data deposition: The data reported in this paper have been deposited in the NOAA National Climatic Data Center.

[1]To whom correspondence may be addressed. E-mail: jochen.halfar@utoronto.ca.

This article contains supporting information online at www.pnas.org/lookup/suppl/doi:10.1073/pnas.1313775110/-/DCSupplemental.

living specimens in the Arctic with life spans of up to 646 y—the oldest continuously growing crustose coralline algae known to date. Annual growth rates of *Clathromorphum* are dependent on both light and temperature (14, 15) and decline slowly with temperature from 400 μm/y near the southern limit of distribution of *C. compactum* at 43°N to 240 μm/y at 52°N, the beginning of significant sea ice (Fig. S1). From that point northwards, even though temperatures continue to decline slowly, growth decreases sharply to 61 μm/y at 73°N. Growth north of 52°N in the western Labrador Sea and Baffin Island region is therefore related to declining solar insolation on the seafloor due to snow-covered sea ice. During the ice-free period, photosynthesis in this species is highly efficient and excess photosynthate is stored (11). With time under sea ice, the stored photosynthates are exhausted, limiting annual growth rates. In addition, water temperatures, which are uniform near −1.8 °C below sea ice under normal marine conditions (16), rise only during the ice-free period. Hence, the length of the annual open water interval, allowing atmospheric and solar heating of surface waters, controls the number of days when sea surface temperatures (SSTs) are above the sea-ice minimum. At the same time, this also determines the number of days available for significant algal growth to take place. The annual SST pattern in turn is preserved as cycles of Mg/Ca ratios in *C. compactum*. In the fall, recording of Mg/Ca ratios stops when growth ceases after the onset of SIC (as reflected by the narrow V-shaped character of the annual Mg/Ca cycle; Fig. S2) and only resumes when algal calcification is reinitiated following sea-ice retreat. Hence, longer ice-free periods, which also allow for more extensive summer sea surface warming, are reflected by higher annually averaged Mg/Ca ratios. Thus, the two variables, growth and annual Mg/Ca ratios, are both proxies for the duration of SIC. Combining both proxies yields a powerful means for SIC reconstructions.

We generated individual algal proxy records by averaging normalized annual growth and Mg/Ca records from live-collected specimens from an Arctic locality characterized by an ice-free period lasting from approximately June to September and a Subarctic locality closer to the southern limit of winter sea-ice extent with an average ice-free season from May through November (Fig. 1). Algal records from both locations are significantly correlated to observational data of SIC from both satellite and ice-chart records from the 1970s onwards (Fig. 2*A*). At the Arctic (Subarctic) locality, up to 39% (38%) of the algal signal (1982–2007) is explained by National Snow and Ice Data Center (NSIDC)-derived SIC, and only 6% (23%) by satellite SST (21). Hence, ice cover is the dominant component driving the algal records. Much of the remaining variability can be attributed to local, as opposed to regional, temperature and particularly ice conditions distinguishing the algal records from the spatially averaged temperature and sea ice observational data (Fig. 1 shows regions used for proxy verification). An averaged record of three individual algal time series from both locations (Fig. S3) yields a long-term relationship to observational SIC data off eastern Canada (19) and the instrumental wintertime NAO for the past 150 y (20) (Fig. 2*B*). Modeling studies have shown that the NAO exerts an influence on the spatial distribution of winter sea ice via wind-driven anomalies of sea-ice velocity, surface vertical heat flux, and possibly horizontal oceanic heat flux (7). There is strong observational evidence connecting Arctic sea-ice distribution with the positive NAO trend from the 1960s to the early 1990s (4). At this time SIC over the Labrador Sea region and eastern Canadian Subarctic was anomalously high due to wind-driven equatorward advection of ice (7, 22), which is reflected by an interval of low growth rates and Mg/Ca ratios in the algal record (Fig. 2*B*). In contrast, the most dramatic increase in algal growth and Mg/Ca anomalies took place during a negative NAO phase starting in the 1920s (Fig. 2*B*) accompanied by strong Arctic warming and sea-ice retreat (5). An

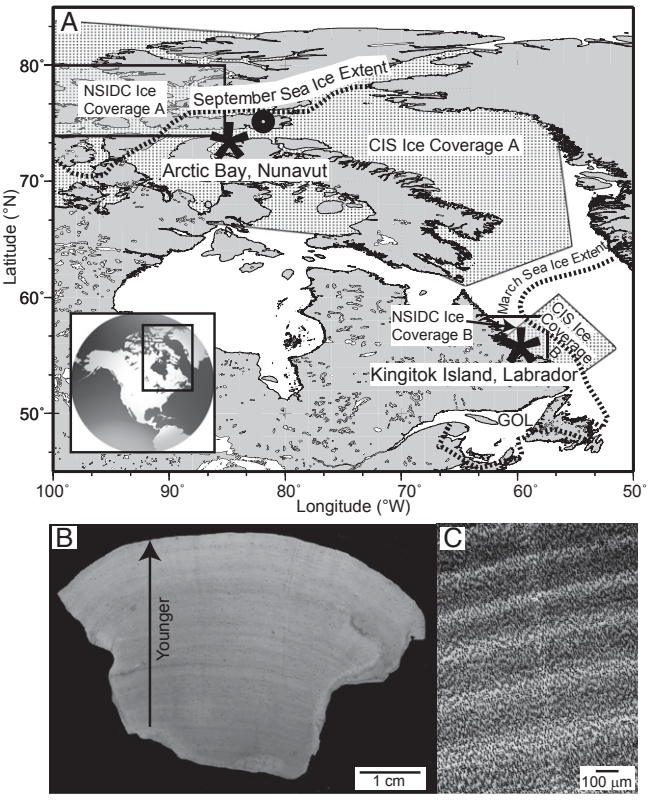

Fig. 1. (*A*) Locations of crustose coralline algal sea-ice proxy records (asterisks) near margins of summer and winter sea-ice extent (1979–2000 average; from NSIDC) (17). In addition, regions used for proxy verification (Fig. 2) are indicated on the map (*Methods*). Black circle indicates location of Devon Island ice core record within close proximity to Arctic Bay algal time series (18). GOL, Gulf of Saint Lawrence. (*B*) Polished slab of live-collected *Clathromorphum compactum* specimen. Specimen lifespan, 240 y. (*C*) Backscattered electron image showing annual growth increments. White dots are individual electron microprobe elemental ratio spot measurements.

accelerated sea-ice decline starting in the 1990s is evident from both the algal proxy time series and observational data (19).

A 646-y long algal reconstruction of sea ice emphasizes the expression of the Little Ice Age (LIA) off eastern Subarctic and Arctic Canada, which is characterized by negative algal anomalies between 1530 and 1860 pointing to extensive SIC (Fig. 3). This is consistent with low Arctic temperatures (23), an increase in SIC as observed in historical accounts from Iceland and the Fram Strait (24, 25), and shown by ice core-based proxy reconstructions from Svalbard and Devon Island (18, 26). In addition, a southward migration of Thule/Labrador Inuit from Hamilton Inlet (54°N) to the northern Gulf of Saint Lawrence during the period 1500–1650 coincided with the LIA-related ice expansion that began in the early 16th century (Fig. 3). That expansion is evidenced by an increase in ice-sensitive harp seal remains found in Labrador middens and the dominance of migratory harp seals in pioneer Inuit settlement middens in the northeastern Gulf of Saint Lawrence (27). Subsistence hunting methods of the Inuit relied on ice access and may have therefore strongly benefited from the regional increase in SIC. In contrast, an overall decrease in Arctic-wide ice cover between the late 15th and early 17th century has been observed in another multiproxy-based study (3). The authors explain the declining SIC during the first half of the LIA by increased advection of warm and saline water into the eastern Arctic Ocean from the North Atlantic, a mechanism that is commonly regarded as a key element of preindustrial Arctic SIC (8). Differences between the Arctic-wide observations

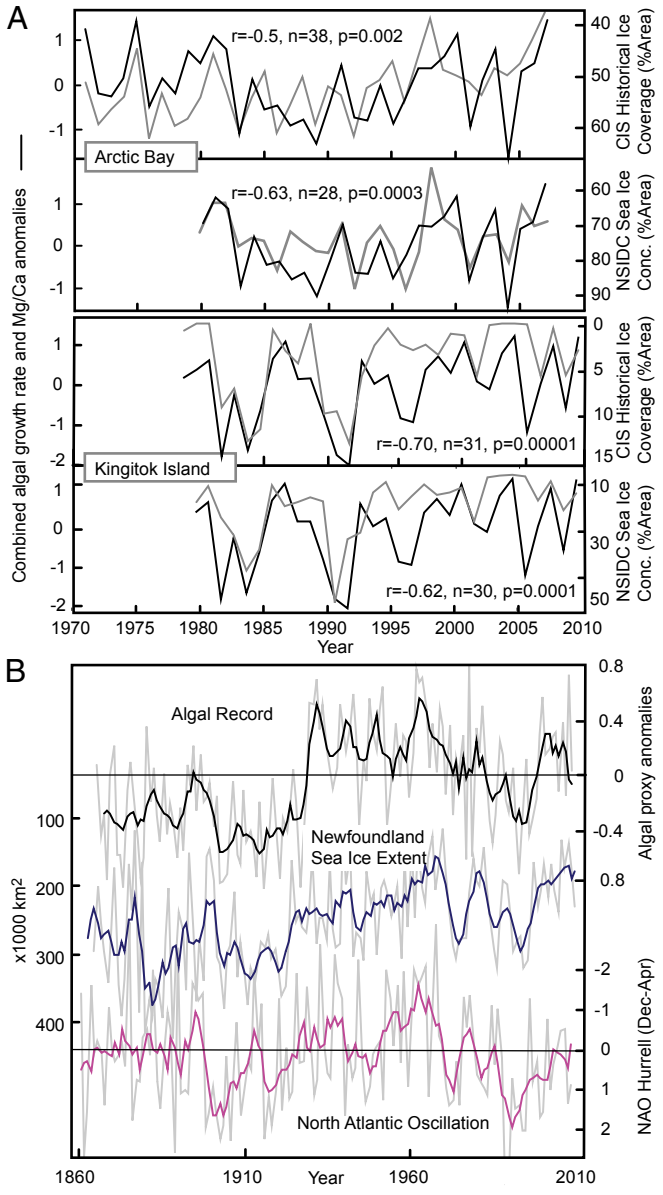

Fig. 2. Relation between sea-ice area coverage observations and crustose coralline algal proxy time series. (*A*) Algal proxy time series for two individual specimens [Arctic Bay (AB1) and Kingitok Island (Ki1)] compared with satellite (NSIDC) and sea-ice chart (CIS) data. Individual time series were calculated by averaging equally weighted normalized annual growth and Mg/Ca ratios of each specimen (see *Methods* for details). NSIDC data shown as July–August average from 1980 to 2007 (Arctic) and 1980–2010 (Labrador) as percent area covered by sea ice in selected region (Fig. 1). CIS data were computed for calendar week 30 and span from 1971 to 2007 in the Arctic and from 1980 to 2010 in Labrador. (*B*) Comparison of algal proxy time series compiled from multiple samples and locations (see *Methods* for details) to observational record of Newfoundland winter sea-ice extent (19) ($r = -0.72$, $n = 144$, $p_{adj} < 0.001$, 5-y average) and instrumental winter NAO data (20) ($r = -0.5$, $n = 144$, $p_{adj} = 0.006$, 5-y average); gray lines represent annual data, thick lines 5-y averages.

and the northeastern Canadian algal SIC record indicate that the regional variability in sea ice observed in recent decades has already existed during the LIA and highlight the asynchrony of the LIA in distinct regions globally (4, 28).

Temporal variability in the algal record can be divided into three time slices (*i*): the pre-LIA portion (1365–1530), exhibiting singular spectrum analysis (SSA) and multitaper method (MTM) spectra with dominant frequencies centered between 43 and 25 y (95% significant), which explain 33% of the variance and frequencies between 3.5 and 5 y (11% of the variance) (Fig. S4); (*ii*) the LIA (1530–1860) is characterized by a combined high-frequency signal at 8 and 5.6 (99% significance, explaining 20% variance) and 37–38 y (95% significance, explaining 15%); and (*iii*) post-1860 multidecadal variability returns to a dominant 45- to 83-y signal (99% significance, explaining 26% of the variance). Thus, whereas multidecadal frequencies dominate the intervals of low SIC, the LIA is characterized by high-frequency variability in sea ice. A more unstable decadal-scale climate and higher-frequency sea-ice variability appear to be a feature of a cold background climate, compared with pronounced multidecadal variability during warmer intervals (29, 30). Hence, with future warming we can expect a continuation of multidecadal sea-ice variability that has dominated the Arctic since 1860. During these past 150 y, the algae have witnessed a sea-ice decline unprecedented in at least the past 646 y.

Methods

Samples of *C. compactum* were live collected at Arctic Bay, Nunavut, Canada (73.0174°N; 85.1536°W, sample AB1, 17-m depth, lifespan 1779–2009) and off Kingitok Island, Labrador, Canada (55.3983°N; 59.8467°W, sample Ki1, 17-m depth, lifespan 1851–2011; sample Ki2, 15-m depth, lifespan 1365–2011). Mg/Ca ratios were measured along transects extending over the entire lifespan of each specimen using a JEOL JXA 8900 RL electron microprobe at the University of Göttingen. For quantitative wavelength dispersive measurements, an acceleration voltage of 10 kV, a spot diameter of 3.5 μm, and a beam current of 12 nA were used. The K-alpha signals of Mg and Ca were simultaneously analyzed for 30 s on two and three spectrometers, respectively. Samples were obtained along transect lines oriented perpendicular to the plane of calcite accretion. Mg/Ca ratios were measured at 15-μm steps for specimens Ki1 and Ki2, and 10-μm steps for specimen AB1. Specimen AB1 is characterized by reduced growth rates due to its high-Arctic location, which necessitated higher-resolution sampling to achieve subannual sampling resolution (average of approximately six samples per year) (Fig. S3 shows individual records). At each interval the specific subsample location was selected manually by moving the stage no more than 20 μm laterally from the transect line to avoid unsuitable sample locations (i.e., conceptacles = reproductive structures and uncalcified cell interiors). The relative mean SDs of multiple standard measurements were found to be no larger than 1.0% for MgO and 1.2% for CaO (2-sigma). Counting statistics errors vary between 1.0 relative percent and 2.9 relative percent for MgO and between 0.40 relative percent and 0.62 relative percent for CaO (2-sigma). All analyzed MgO concentrations clearly exceed the detection limit, which, calculated from the background noise, was 0.015% (2-sigma). Age models were established based on the pronounced seasonal cycle in algal Mg/Ca as discussed in Halfar et al. (14). Maximum (minimum) Mg/Ca values of subannual cycles were tied to August (March), which is on average the warmest (coolest) month in the study area. Minimum Mg/Ca values represent the winter growth break, which was assigned to the maximum extent of the sea-ice season (March). Mg/Ca time series were linearly interpolated between these anchor points using AnalySeries software (31) to obtain an equidistant proxy time series with 12 samples per year resolution. The developed chronology was refined and thoroughly cross-checked for possible errors in the age model by comparing annual extreme values in the Mg/Ca ratio time series to imaged growth increment patterns for each individual year of algal growth. In addition, the age model was confirmed by three accelerator mass spectrometry (AMS) radiocarbon dates obtained from sample Ki2 (Fig. 3 shows position of dates and Table S1, analytical details). Once an age model was finalized, annual average Mg/Ca ratios were calculated from the 12 samples per year dataset. In addition, widths of annual Mg/Ca cycles were determined by calculating the distance between microprobe stage coordinates of successive Mg/Ca lows. Widths of annual Mg/Ca cycles are equivalent to annual vertical growth rates (14). Error of growth measurement is dependent on microprobe sampling resolution (e.g., 15 μm for Ki1 and Ki2, 10 μm for AB1). As collections took place during the summer months, the year of collection is incomplete and counting was done starting from the year before collection. Individual reconstructions were standardized to have a mean of zero and unit variance. A combined algal record (Fig. 3) was calculated by averaging the normalized annual growth rates and annually averaged Mg/Ca ratios from all three samples, giving equal weight to each of the time series (Fig. S3 shows individual records). Regions used for proxy calibration (Fig. 2*A*): NSIDC ice coverage time series were obtained as summer average (July–August) of sea-ice concentrations

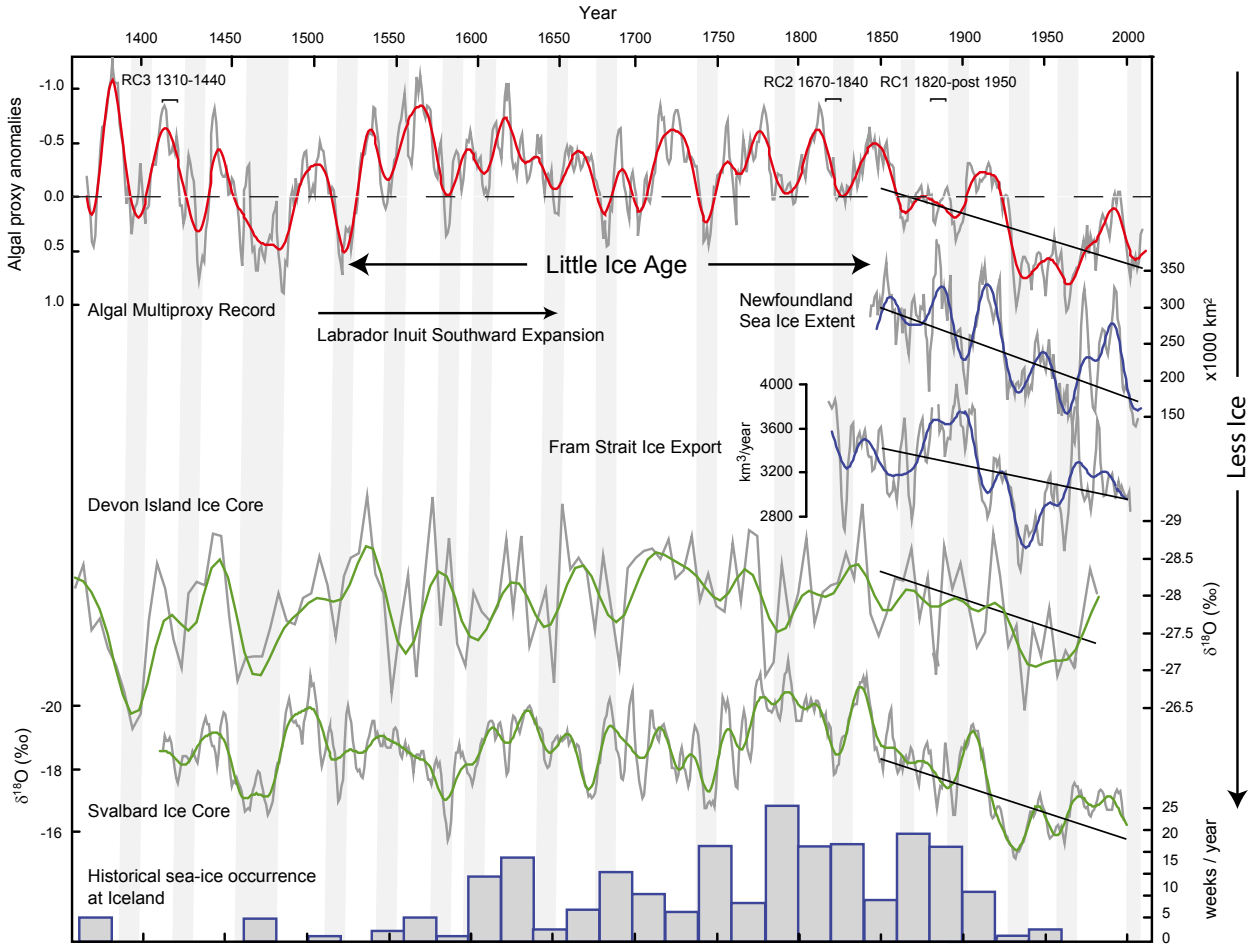

Fig. 3. Algal proxy record (red) compared with observational (blue) and proxy (green) data (see *Methods* for detail on records). Gray lines represent 5-y moving average and colored lines, 15-y low-pass filtered (Savitzky–Goley) annual data. Algal proxy time series plotted on inverted scale to indicate declining ice cover. Light gray bars show periods of positive algal anomalies, reflected by negative ice anomalies in observational records, and positive $\delta^{18}O$ ice core excursions. Linear trends for all time series are plotted from 1850 onwards. All individual algal specimens yield similar trends (Fig. S3). RC indicates position of radiocarbon analyses. Values are 2σ calibrated results (Table S1); all values fall well within age model derived from growth increment counting.

derived from satellite brightness data (17). NSIDC regions were selected based on spatial correlations of proxy records with ice-coverage data. Region A encompasses 74–80°N, 85–100°W; region B encompasses 54–57°N, 57–62°W. Canadian Ice Service (CIS) time series were compiled from weekly regional ice charts from predefined regions (A, northern Canadian water; B, southern Labrador) using Ice Graph (32). SST data were obtained from Reynolds et al. (21). Newfoundland winter sea-ice extent (Fig. 2*B*) was derived from historical and observational records (19). Historical observations and modeled data of Fram Strait ice export from Schmith and Hansen (24). Svalbard Austfonna $\delta^{18}O$ ice core record has been interpreted as sea-ice extent proxy (26), whereas Devon Island ice core $\delta^{18}O$ record (Fig. 1 for location) shows correlation with sea-ice conditions at decadal timescales only (3). Historical record of sea-ice occurrence off Iceland was modified from Lamb (25).

ACKNOWLEDGMENTS. W. Kuhs stimulated our interest in ice-cover proxy development. Funding was provided by Estech (Ecological Systems Technology) (to W.H.A.), National Science and Engineering Research Council (to J.H. and E.E.), a Canadian Foundation for Climate and Atmospheric Sciences Grant (to J.H.), an ArcticNet Network of Centres of Expertise Grant (to E.E.), and the Smithsonian Institution (to W.H.A. and W.W.F.).

1. de Vernal A, Gersonse R, Goosse H, Seidenkrantz M-S, Wolff EW (2013) Sea ice in the paleoclimate system: The challenge of reconstructing sea ice from proxies—an introduction. *Quat Sci Rev*, 10.1016/j.quascirev.2013.08.009.
2. Abram NJ, Wolff E, Curran MAJ (2013) A review of sea ice proxy information from polar ice cores. *Quat Sci Rev*, 10.1016/j.quascirev.2013.01.011.
3. Kinnard C, et al. (2011) Reconstructed changes in Arctic sea ice over the past 1,450 years. *Nature* 479(7374):509–512.
4. Grumet N, et al. (2001) Variability of sea-ice extent in Baffin Bay over the last millennium. *Clim Change* 49:129–145.
5. Semenov VA, Bengtsson L (2003) Modes of the wintertime Arctic temperature variability. *Geophys Res Lett* 30(15):1781–1784.
6. Rodrigues J (2008) The rapid decline of sea ice in the Russian Arctic. *Cold Reg Sci Technol* 54(2):124–142.
7. Strong C, Magnusdottir G (2010) Modeled winter sea ice variability and the North Atlantic Oscillation: A multi-century perspective. *Clim Dyn* 34:515–525.
8. Spielhagen RF, et al. (2011) Enhanced modern heat transfer to the Arctic by warm Atlantic Water. *Science* 331(6016):450–453.
9. Gersonde R, de Vernal A (2013) Reconstruction of past sea ice extent. PAGES News 21 (1):30–31.
10. Polyak L, et al. (2010) History of sea ice in the Arctic. *Quat Sci Rev* 29:1757–1778.
11. Adey WH, Halfar J, Williams B (2013) The coralline genus *Clathromorphum* Foslie emend. Adey: Biological, physiological, and ecological factors controlling carbonate production in an Arctic-Subarctic climate archive. *Smithsonian Contributions to the Marine Sciences* (Smithsonian Institution Scholarly Press, Washington, DC), Vol 40, pp 1–48.
12. Halfar J, Steneck RS, Joachimski M, Kronz A, Wanamaker AD, Jr. (2008) Coralline red algae as high-resolution climate recorders. *Geology* 36:463–466.
13. Hetzinger S, et al. (2012) First proxy evidence linking decadal North Pacific and Atlantic climate. *Clim Dyn* 39(6):1447–1455.
14. Halfar J, et al. (2011) Coralline algal growth-increment widths archive North Atlantic climate variability. *Palaeogeogr Palaeoclimatol Palaeoecol* 302:71–80.
15. Halfar J, et al. (2011) 225 years of Bering Sea climate and ecosystem dynamics revealed by coralline algal growth-increment widths. *Geology* 39(6):579–582.
16. Reynolds RW, Smith TM (1994) Improved global sea surface temperature analyses using optimum interpolation. *J Clim* 7:929–948.

17. Meier W, Fetterer F, Knowles K, Savoie M, Brodzik MJ (2006, updated quarterly) Sea ice concentrations from Nimbus-7 SMMR and DMSP SSM/I passive microwave data (National Snow and Ice Data Center, Boulder, CO), 1980–2011.
18. Kinnard C, Zdanowicz CM, Fisher DA, Wake CP (2006) Calibration of an ice-core glaciochemical (sea-salt) record with sea-ice variability in the Canadian Arctic. *Ann Glaciol* 44:383–390.
19. Hill BT, Jones SJ (1990) The Newfoundland ice extent and the solar cycle from 1860 to 1988. *Journal of Geophysical Research* 95:5385–5394.
20. Hurrell JW (1995) Decadal trends in the North Atlantic Oscillation: Regional temperatures and precipitation. *Science* 269(5224):676–679.
21. Reynolds RW, Rayner NA, Smith TM, Stokes DC, Wang W (2002) An improved in situ and satellite SST analysis for climate. *J Clim* 15:1609–1625.
22. Chapman WL, Walsh JE (1993) Recent variations of sea ice and air temperature in high latitudes. *Bull Am Meteorol Soc* 74(1):33–47.
23. Kaufman DS, et al.; Arctic Lakes 2k Project Members (2009) Recent warming reverses long-term arctic cooling. *Science* 325(5945):1236–1239.
24. Schmith T, Hansen C (2003) Fram Strait ice export during the nineteenth and twentieth centuries reconstructed from a multiyear sea ice index from southwestern Greenland. *J Clim* 16:2781–2791.
25. Lamb HH (1977) Climate history and the future. *Climate: Present, Past and Future* (Methuen, London), Vol 2.
26. Isaksson E, et al. (2005) Two ice-core $d^{18}O$ records from Svalbard illustrating climate and sea-ice variability over the last 400 years. *Holocene* 15:501–509.
27. Fitzhugh WW (2006) Cultures, borders, and basques: Archaeological surveys on Quebec's lower north shore. *From the Arctic to Avalon: Papers in Honour of James A Tuck Jr.*, eds Rankin L, Ramsden P, British Archaeological Reports International Series (Archaeopress, Oxford, London), 1507:53–70.
28. Ahmed M; PAGES 2k Consortium (2013) Continental-scale temperature variability during the past two millennia. *Nature Geosc* 6:339–346.
29. Chylek P, Folland CK, Dijkstra HA, Lesins G, Dubey MK (2011) Ice-core data evidence for a prominent near 20 year time-scale of the Atlantic Multidecadal Oscillation. *Geophys Res Lett* 38:L13704.
30. Kobashi T, et al. (2009) Persistent multi-decadal Greenland temperature fluctuation through the last millennium. *Clim Change* 100:733–756.
31. Paillard D, Labeyrie L, Yiou P (1996) Macintosh program performs time-series analysis. *Eos Trans AGU* 77:379.
32. Tivy A, et al. (2011) Trends and variability in summer sea ice cover in the Canadian Arctic based on the Canadian Ice Service Digital Archive. *J Geophys Res* 116(C03007): 10.1029/2009JC005855.

Supporting Information

Halfar et al. 10.1073/pnas.1313775110

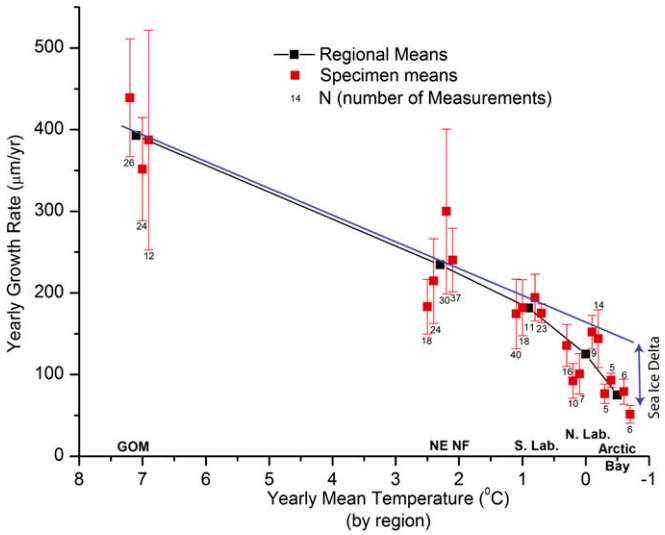

Fig. S1. Annual growth rates across latitudes. Regional yearly growth rates of *Clathromorphum compactum* as a function of sea surface temperature (SST) in the northwestern North Atlantic, Labrador Sea, and Arctic Bay, northern Baffin Island. Growth rates analyzed from scanning electron microscope images and Mg/Ca cycle widths (Fig. S3); error bars show SD. The red squares are individual specimens. Satellite-derived SST data for each locality were obtained from Reynolds et al. (1). Growth rate decline is uniform from the Gulf of Maine (GOM) at 43°N northwards to 52°N (northern Newfoundland (NE NF). From that point, even though temperatures continue to decline slowly, growth declines sharply to 61 µm/y at 73°N (Arctic Bay). This results in a significant departure from the linear relationship of growth and temperature. A linear relationship not only exists for *C. compactum* south of 52°N, but was also experimentally determined for several Subarctic coralline species (2). If sea-ice cover persists for more than 2 mo, growth ceases, likely due to lack of sufficient stored photosynthate. Growth north of 52°N in the western Labrador Sea and Baffin Island region is therefore related to declining solar insolation on the seafloor due to snow-covered sea ice (marked as sea ice delta; blue line) (SE NF, southeastern Newfoundland; S. Lab, southern Labrador; N. Lab, Northern Labrador; modified from Adey et al. (3). Light attenuation of sea ice can vary according to age of ice (multi- or single-year ice), thickness, ice type, snow cover, meltwater ponds, and growth of ice-algal mats. However, even assuming thin (~1 m) single-year blue ice without snow cover and ice algae, photosynthetically active radiation (PAR)-spectrum light penetration is only about 30% (4). Considering fall and winter darkness, this results in highly limited amounts of light reaching the seafloor. By the time spring light conditions return, snow cover, white ice, and meltpond formation will have additionally reduced transparency of the sea ice. Specimens of *C. compactum* used in this study were collected between 15- and 17-m water depth, which is near the lower limit of distribution of this species (3). Hence, it can be assumed that any type of sea-ice condition will be sufficient to provide low-enough amounts of light to the seafloor to inhibit photosynthetic activity and therefore significant calcification in *C. compactum* during periods of sea-ice coverage.

1. Reynolds RW, Rayner NA, Smith TM, Stokes DC, Wang W (2002) An improved in situ and satellite SST analysis for climate. *J Clim* 15:1609–1625.
2. Adey WH (1970) The effects of light and temperature on growth rates in boreal-subarctic crustose corallines. *J Phycol* 6:269–276.
3. Adey WH, Halfar J, Williams B (2013) The coralline genus *Clathromorphum* Foslie emend. Adey: Biological, physiological, and ecological factors controlling carbonate production in an Arctic-Subarctic climate archive. *Smithsonian Contributions to the Marine Sciences* (Smithsonian Institution Scholarly Press, Washington, DC), Vol 40, pp 1–48.
4. Maykut GA, Grenfell TC (1975) The spectral distribution of light beneath first-year sea ice in the Arctic Ocean. *Limnol Oceanogr* 20(4):554–563.

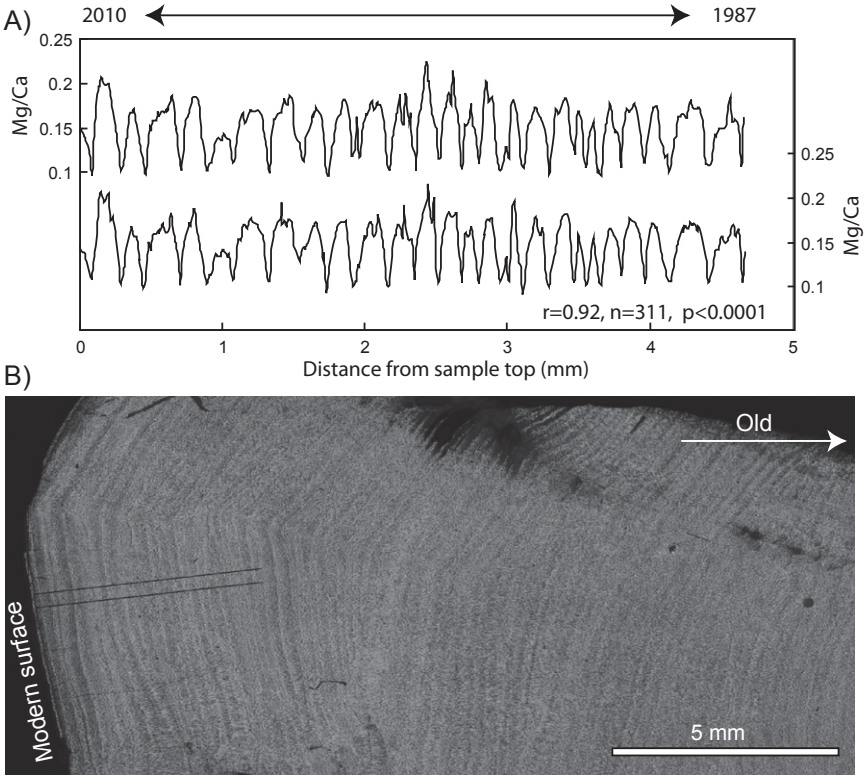

Fig. S2. Analytical reproducibility. Annual cycles of Mg/Ca ratios measured by electron microprobe (*A*) on two parallel transects along main axis of growth on uppermost 5 mm of sample Ki2 (*B*). Microscope image of polished sample shows ~80 annual growth increments. Cycle shapes in *A* are characteristic of break in growth during sea-ice season, with narrow downward pointing peak. Summer portions of cycles instead are smooth, reflecting summer light and temperature cycle patterns following spring breakup of sea ice. Note similarity of winter Mg/Ca ratios reflecting constant seawater temperature under sea ice. Sample spacing, 15 μm (average annual growth of Ki2 = 172 μm) results in average resolution of ~11.5 samples per year. Mg/Ca ratios are based on atom percent of Mg and Ca.

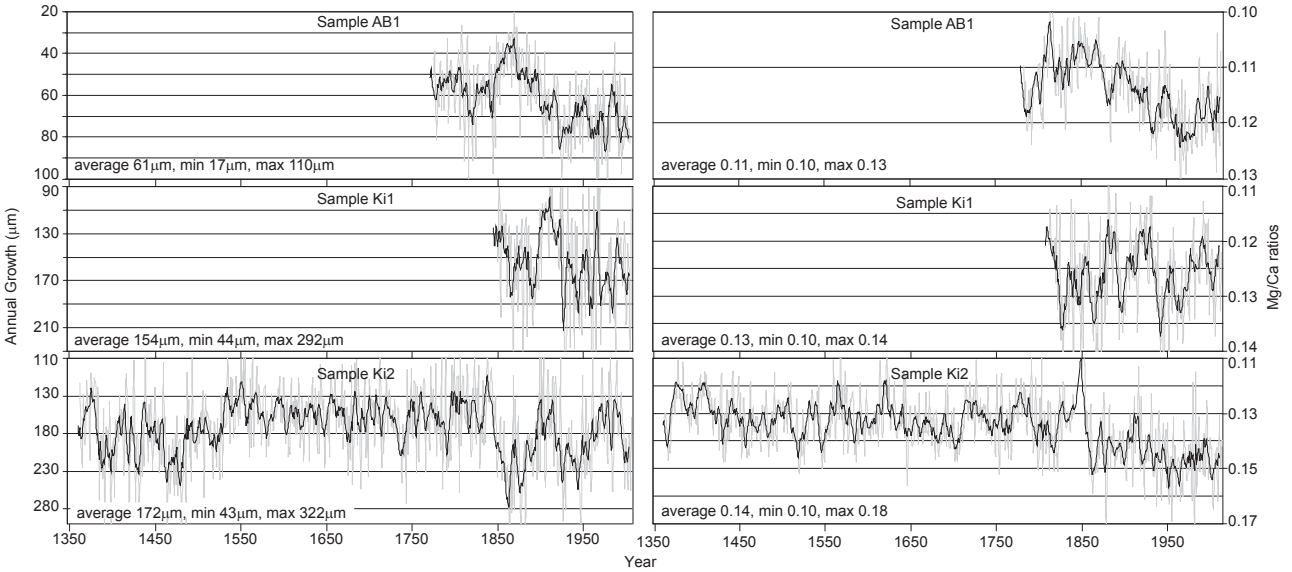

Fig. S3. Annual growth and Mg/Ca ratios of individual samples. Gray lines show annual data, black lines indicate five-point moving average. Note that in accordance with Fig. 3, *y* axes values are plotted in reverse order. A common trend toward increasing growth and higher Mg/Ca ratios (= less sea-ice) is apparent from the mid-19th century onwards. Using the individual records shown here, a combined algal growth increment width and Mg/Ca ratio time series was calculated by averaging equally weighted normalized time series (Fig. 3). Combining multiple proxy records from various locations reduces local and sample-specific variability as has been demonstrated before for coralline algae (1).

1. Halfar J, et al. (2011) Coralline algal growth-increment widths archive North Atlantic climate variability. *Palaeogeogr Palaeoclimatol Palaeoecol* 302:71–80.

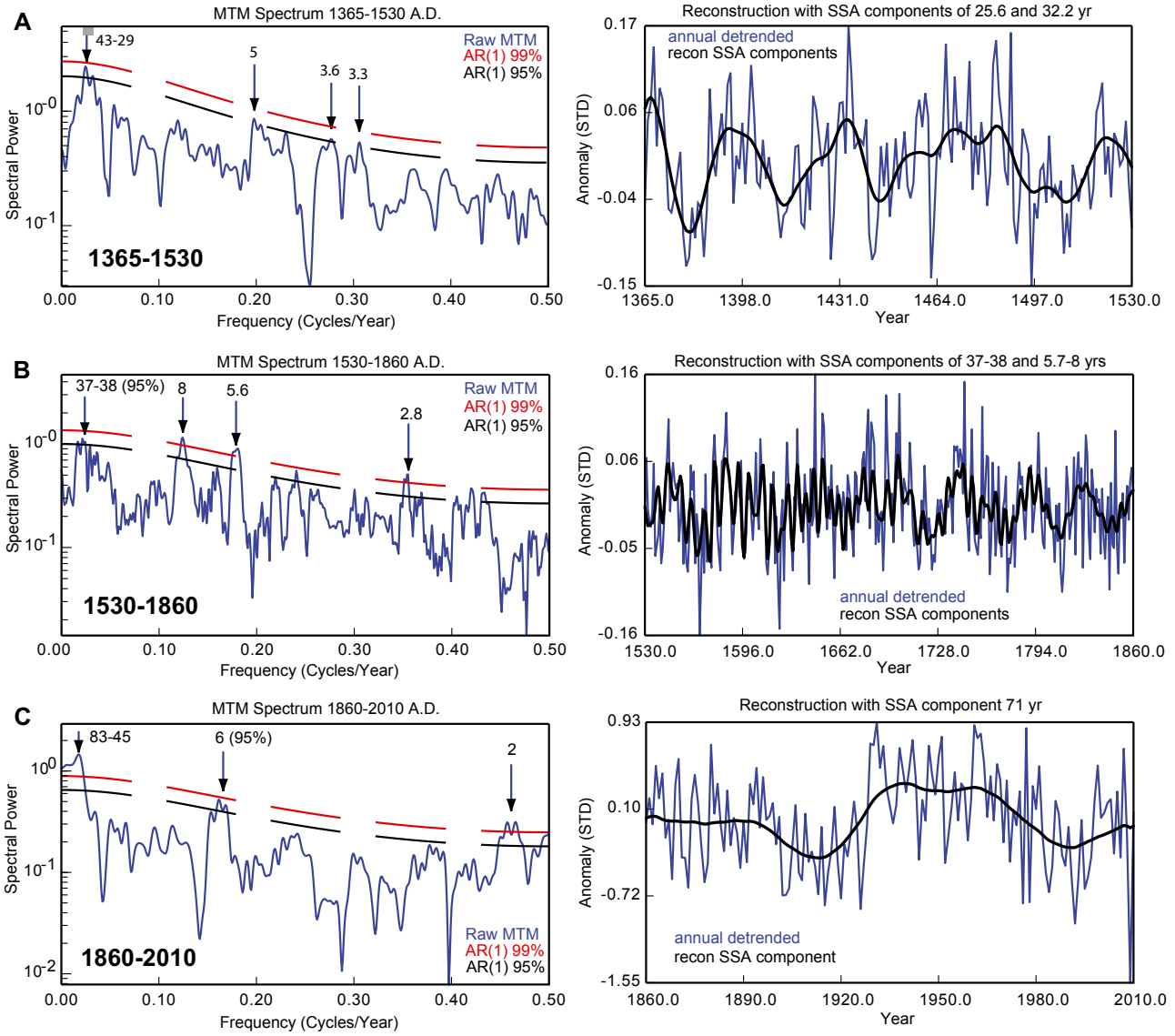

Fig. S4. Spectral analysis of annually averaged algal time series for (*A*) 1365–1530, (*B*) 1530–1860, and (*C*) 1860–2010 time intervals. Periods (years) of peaks significant at the 95/99% level are indicated (multitaper method, MTM, *Left*). The significance estimates in the MTM are independent of the spectral power. (*Right*) Annual detrended algal time series (blue) and dominant reconstructed singular spectrum analysis (SSA) components (black). For spectral analysis of coralline algal data the SSA–MTM Toolkit (1) was used. Before spectral analysis, time series were normalized to unit variance and detrended by removing the linear trend. The MTM (*Left*) was applied, which provides useful tools for spectral estimation (1) and signal reconstruction with high spectral resolution and significance tests. The significance tests are independent of the spectral power, therefore even oscillations with small amplitudes can be identified with a high significance level in a time series whose spectrum may contain both broadband and line components (1). Using the MTM, a small set of data tapers, or data windows, is applied to the data in the time domain to reduce the variance of spectral estimates before Fourier transformation (2). This method has been widely used for problems in geophysical signal analysis, for example analyses of instrumental data of the atmosphere and ocean, and paleoclimate proxy data (2, 3). A detailed description of this method can be found in Ghil et al. (1).

1. Ghil M, et al. (2002) Advanced spectral methods for climatic time series. *Rev Geophys* 40(1):1–41.
2. Thompson DJ (1982) Spectrum estimation and harmonic analysis. Institute of Electrical and Electronics Engineers Proceedings (Institute of Electrical and Electronics Engineers, Washington, DC), 70(1055–1096).
3. Mann ME, Lees J (1996) Robust estimation of background noise and signal detection in climatic time series. *Clim Change* 33:409–445.

Table S1. Results from AMS radiocarbon dating of sample Ki2

Sample	Measured age, B.P.	$^{13}C/^{12}C$, ‰	Conventional age, B.P.	2σ calibration	Expected*
RC1	140 ± 30	−2.0	520 ± 30	Cal AD 1820–post-1950	1875–1880
RC2	240 ± 30	+0.5	660 ± 30	Cal AD 1670–1840	1815–1825
RC3	670 ± 30	0.0	1080 ± 30	Cal AD 1310–1440	1435–1445

Samples were measured by Beta Analytics, Inc. Expected, age determined by age model based on growth increments and Mg/Ca cycles (Fig. S2). RC, radiocarbon sample; Cal AD, calibrated anno domini.
*Age determined.